processes

MDPI

Article

Experimental and Kinetic Modeling Study on the Autoignition of Ammonia/Propane Mixtures

Weixian Ma [1,2,†], Danyang Guo [2,3,†], Hua Xiao [2,*], Aiguo Chen [2], Jun Li [2,*], Yuhong Nie [2], You Gong [2] and Changhong Wang [1]

[1] School of Materials and Energy, Guangdong University of Technology, Guangzhou 510006, China; maweixian1998@163.com (W.M.); wangchh@gdut.edu.cn (C.W.)
[2] School of Ocean Engineering, Guangzhou Maritime University, Guangzhou 510725, China; guodanyang11@163.com (D.G.); chenaiguo@gzmtu.edu.cn (A.C.); nieyh@gzmtu.edu.cn (Y.N.); gongyou@gzmtu.edu.cn (Y.G.)
[3] College of Vehicle and Traffic Engineering, Henan University of Science and Technology, Luoyang 471003, China
* Correspondence: xiaohua@gzmtu.edu.cn (H.X.); junli0201@163.com (J.L.)
† These authors contribute equally to this work.

Abstract

Utilizing ammonia (NH_3) as a zero-carbon alternative fuel requires a deeper understanding of its combustion characteristics, with ignition delay time (IDT) serving as a critical descriptive parameter. To investigate the effects of propane (C_3H_8) addition on NH_3 ignition at high temperatures, the ignition delay times of NH_3/C_3H_8 blends were systematically measured using a shock tube over a wide range of conditions: temperatures of 1263–2117 K, pressures of 0.14–0.5 MPa, equivalence ratios of 0.5–2.0 and propane mole fractions of 5–70%. The results indicate that propane addition significantly promotes ammonia ignition. Under stoichiometric and 1.4 atm pressure conditions, the addition of C_3H_8 to pure NH_3 reduces the ignition delay time by approximately fivefold, allowing auto-ignition to occur at a lower temperature. Furthermore, detailed chemical kinetic mechanisms from the literature were adopted for numerical simulations and validated against the newly acquired experimental data. Kinetic analysis reveals that the propane addition does not alter the main oxidation pathways of ammonia, while it triggers C-N cross-reactions at higher blending ratios (>30%). The active radicals generated during the early stages of propane oxidation accelerate H-abstraction reactions, serving as the key mechanism responsible for the shortened ignition delay times and promoted ignition.

Keywords: ammonia; propane; shock tube; ignition delay time; chemical kinetics

Check for updates

Academic Editor: Codina Movileanu

Received: 18 August 2026
Revised: 10 September 2026
Accepted: 12 September 2026
Published: 16 September 2026

Copyright: © 2026 by the authors. Licensee MDPI, Basel, Switzerland. This article is an open access article distributed under the terms and conditions of the Creative Commons Attribution (CC BY) license.

1. Introduction

Ammonia, as an emerging carbon-neutral fuel, has attracted widespread attention in the energy and power sectors in recent years. Containing no carbon in its molecule, its combustion process does not produce carbon dioxide, making it a potential clean energy carrier in the context of achieving the carbon neutrality goals [1–3]. Furthermore, ammonia can be synthesized via electrolysis of water, electrochemical processes, or photocatalytic conversion using renewable energy sources [4,5], and it can be easily liquefied for storage and transportation, offering compatibility with existing infrastructure for replacing conventional fossil fuels. However, when used as a sole fuel, ammonia faces challenges such as low burning velocity, high ignition energy, narrow flammability limits, and poor flame

stability [6], primarily due to its high auto-ignition temperature and long IDT. To improve its combustion performance, current research has explored blending NH_3 with fuels such as diesel [7,8], hydrogen [9], methane [10,11], dimethyl ether [12,13], and alcohols [14–16], demonstrating that these mixtures can promote the ignition/combustion performance of ammonia.

Propane is a widely utilized hydrocarbon fuel and a primary component of liquefied petroleum gas. It exhibits well-established chemical reaction pathways, high burning velocity, very low ignition energy, and broad flammability limits. Existing literature includes several studies on ammonia/propane blended fuels. Yin et al. [17] conducted experimental studies in a jet-stirred reactor, focusing on the oxidation kinetics of ammonia-propane mixtures. The experiments were performed over a temperature range of 800–1250 K and equivalence ratios from 0.5 to 2.0, investigating the effect of propane volume fraction (0.2–0.8) by analyzing the mole fractions of intermediate species. The research team developed a new kinetic mechanism for ammonia-propane blends, which accurately predicts the experimental data under various conditions. Yin et al. [18] further measured the laminar flame speeds of ammonia/propane/air mixtures under conditions of 1–5 atm, 298–453 K, equivalence ratios of 0.7–1.6, and propane fractions ranging from 0% to 90% of the fuel volume. The experimental data validated the effectiveness of the previously developed kinetic model, and comparisons demonstrated that this chemical kinetic mechanism can reasonably predict experimental data for propane, ammonia, and their mixtures under a wide range of conditions. Cheng et al. [19] studied the co-combustion characteristics and nitrogen oxide emissions of ammonia/propane blends at three mixing ratios: pure ammonia, and blends with 5% and 10% propane. They investigated the effects of the ammonia-to-propane ratio, excess air coefficient, and inlet oxygen concentration on combustion and NO_X emission characteristics. The results indicated that as the propane proportion increased, the concentrations of NO_X, NO, and NO_2 rose, while the oxygen concentration decreased. Chen et al. [20] utilized ozone addition to elucidate the flame-enhancement mechanism based on plasma-assisted combustion, investigating through experiments and numerical simulations the effect of ozone addition on the laminar burning velocities of $NH_3/(35\%O_2/65\%N_2)$ and NH_3 + $CH_4/C_2H_6/C_3H_8$ + air flames over a wide range of equivalence ratios. The study shows that blending ammonia with hydrocarbon fuels can reduce ignition energy and increase the overall burning velocity of the mixture. Wang et al. [21] systematically measured the laminar burning velocities of NH_3/C_3H_8/air mixtures at different equivalence ratios (0.6–1.4), ammonia blending ratios (20%, 50%, 80%), and initial pressures (0.1–0.5 MPa). The results showed that propane can significantly enhance the combustion intensity of ammonia, while the addition of ammonia effectively reduces CO and CO_2 emissions. Liu et al. [22] measured the IDTs of stoichiometric NH_3/C_3H_8 mixtures with varying propane fractions (0–30%) using a shock tube under conditions of 1305–1890 K and pressures of 1.75 and 10 bar. They developed a new NH_3-C_3H_8 kinetic model based on an optimized NH_3 model and the C_3H_8 sub-mechanism from NUIG 1.1. The study found that the newly introduced C/N cross-reactions play a crucial role in accurately predicting the ignition, flame propagation, and species profiles of NH_3/C_3H_8 blends. Nobakht et al. [23] measured soot volume fraction, temperature, and soot maturity index in propane/ammonia diffusion flames with varying ammonia addition ratios (fuel mole fraction 0–0.6) at pressures of 1–6 atm, using a co-flow laminar diffusion burner in a high-pressure combustion chamber, combined with multi-wavelength extinction and spectral emission diagnostics. The study systematically investigated the effects of pressure on soot formation and maturity in ammonia/propane mixtures. Experimental results show that ammonia addition reduces soot volume fraction and soot yield at all pressures, but the relative reduction diminishes with increasing pressure. Meanwhile,

the influence of pressure on soot maturity is non-monotonic: at low pressures (1–3 atm), ammonia decreases soot maturity, whereas at high pressures (4–6 atm), this trend weakens or even reverses, leading to a phenomenon where soot mass is reduced but maturity is enhanced. Lin et al. [24] measured the IDTs of ammonia/propane blends with ammonia energy shares of 35% and 70% using a shock tube at stoichiometric conditions, 1 atm, and temperatures from 1200 to 1800 K. Combined with species concentration data obtained from a jet-stirred reactor and chemical kinetic simulations, they systematically investigated the auto-ignition characteristics of ammonia/propane mixtures. The experimental results indicated that the addition of ammonia had only a minor effect on the IDTs of the blends, and that propane exerted a weaker promoting effect on the overall reactivity of natural gas compared with ethane. The developed kinetic model showed good agreement with the experimental data. Liang et al. [25] investigated the auto-ignition characteristics of ammonia/propane blended fuels under high-pressure conditions. Using a rapid compression machine, they measured the IDTs for mixtures with different propane fractions (10–100%) at 750–1100 K and 20–100 bar. Based on the POLIMI-2023 and Aramco 3.0 models, they developed the SJTU-2025 kinetic mechanism.

Although the ignition characteristics of NH_3/C_3H_8 blends have been investigated under a range of conditions, the available experimental database remains limited in terms of fuel composition, equivalence ratio, and temperature–pressure coverage (Table 1). Existing studies have mainly considered moderate C_3H_8 blending ratios (10–50%) and lean-to-stoichiometric conditions, while data for extreme C_3H_8 blending ratios and fuel-rich mixtures remain scarce. In addition, the combined effects of C_3H_8 blending ratio and equivalence ratio on NH_3/C_3H_8 ignition behavior have not been systematically examined over a broad temperature range under low-to-intermediate pressure conditions. These limitations hinder a comprehensive understanding of the competition between NH_3 and C_3H_8 oxidation chemistry and its influence on ignition characteristics. To address these gaps, this study systematically measured the IDTs of NH_3/C_3H_8 mixtures over a wide parameter range (T = 1263–2117 K, p = 0.14 and 0.5 MPa, φ = 0.5, 1.0, and 2.0, with C_3H_8 blending ratios of 5%, 30%, and 70%). The selected fuel compositions and equivalence ratios extend the available database toward extreme C_3H_8 blending and fuel-rich conditions, while the broad temperature range enables the ignition behavior to be examined across different kinetic regimes. Detailed kinetic simulations were further performed to evaluate representative mechanisms and elucidate the competitive reaction pathways governing the ignition behavior.

Table 1. Published experimental studies of the IDTs of NH_3/C_3H_8 mixtures.

Experimental Type	Experimental Settings				References
	C_3H_8/Fuel (%)	T (K)	φ	P (bar)	
Shock tube	0, 10, 20, 30	1303–1890	1.0	1.75–10	Liu 2024 [22]
Shock tube	30, 65, 100	1200–1800	1.0	1.0	Lin 2026 [24]
RCM	10, 30, 50	750–1100	0.5–1.0	20–100	Liang 2026 [25]
Shock tube	5, 30, 70	1263–2117	0.5–2.0	1.4,5.0	This work

2. Experiment Methods

The experiments were conducted on a shock-tube platform as illustrated in the Figure 1. The platform consists of three main components: a stainless-steel tube assembly, a gas-preparation system, and a photoelectric detection system. The main shock tube is constructed from stainless-steel pipe with an inner diameter of 100 mm and a wall thickness of 17.5 mm. To minimize boundary-layer effects, the inner wall of the shock tube was finished to a roughness of less than 0.8 μm. The tube is divided into a 4 m-long driver

section and a 5.5 m-long driven section, separated by a polyethylene terephthalate (PET) diaphragm. Further details of the experimental setup can be found in references [26,27]. The calculation of state parameters of fluid in an ideal shock tube has been added to the Supplementary Materials.

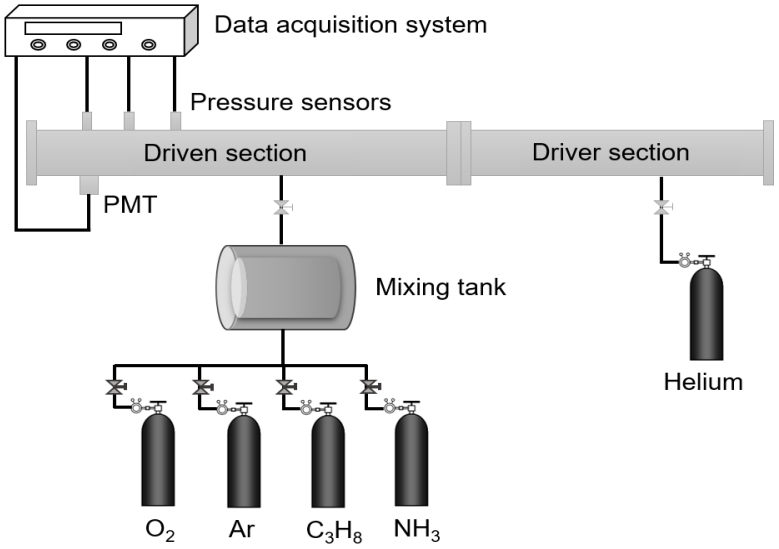


Figure 1. Schematic representation of shock tube.

Three pressure sensors (PCB113B24) were installed at equal intervals (200 mm) along the sidewall of the low-pressure test section. The measured pressure signals were fed into an oscilloscope via a preamplifier. The chemiluminescence optical signal passed through an optical filter and entered a photomultiplier tube (PMT, Hamamatsu CR131) equipped with a high-voltage power supply, allowing the OH* spontaneous emission signal to be transmitted to the oscilloscope. The IDT is defined as follows: the arrival of the reflected shock wave at PCB3 is taken as time zero, and the intersection point of the tangent at the position of maximum slope of the OH signal with the horizontal baseline is taken as the ignition timing, which is the IDT. As shown in Figure 2, the IDT of the 70%NH_3/30%C_3H_8 mixture under the conditions of T = 1392 K, p = 0.14 MPa, and $\varphi = 1.0$ is 1180 μs. The uncertainty in temperature measurement is approximately ±15 K. The experimental IDT data were determined based on the distribution of results from a series of measurements, with a maximum single-measurement error of ±20%. (The detailed uncertainty analysis has been submitted in the Supplementary Materials.)

The driver gas consisted of a helium–nitrogen mixture with a purity of 99.999%. The diluent gas was argon with a purity of 99.999% (dilution ratio: 80%), and the Ar oxidizing environment was simulated using a mixture of 79% argon and 21% oxygen (molar ratio). The test fuel was a premixed gas prepared from high-purity ammonia (99.99%) and propane (99.99%). To mitigate the characteristic adsorption of ammonia on stainless steel surfaces—which could introduce experimental errors—the inner wall of the shock tube was passivated with pure ammonia prior to each measurement. This study investigated nine different test conditions of ammonia/propane mixtures; the specific compositions are listed in Table 2. Furthermore, with $\varphi = 1.0$, additional experiments were conducted at a pressure of 0.5 MPa to thoroughly investigate the influence of pressure on IDT. The selected pressures represent near-atmospheric and moderately elevated pressure conditions, respectively, enabling the pressure dependence of NH_3/C_3H_8 ignition characteristics to be examined under experimentally reliable conditions.

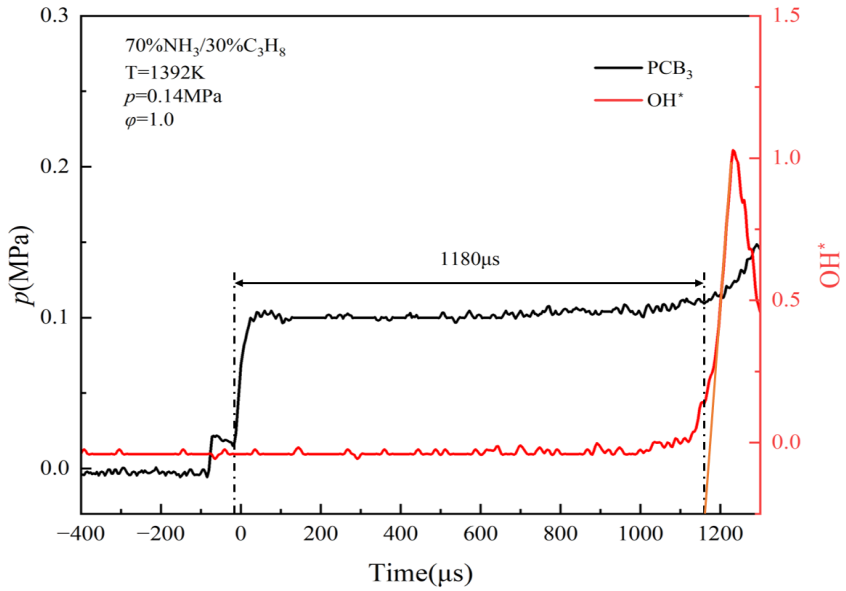


Figure 2. Definition of ignition delay time.

Table 2. Experimental mixtures (unit: mole/%).

	Mixtures	φ	Propane /Fuel	NH_3 (%)	C_3H_8 (%)	O_2 (%)	Ar (%)	*p* (MPa)
1	N95C5	0.5	5%	1.86885	0.09836	3.78689	94.24590	0.14
2	N70C30	0.5	30%	0.69014	0.29577	3.99296	95.02113	0.14
3	N30C70	0.5	70%	0.16449	0.38381	4.08486	95.36684	0.14
4/5	N95C5	1.0	5%	3.40299	0.17910	3.44776	92.97015	0.14/0.5
6/7	N70C30	1.0	30%	1.31544	0.56376	3.80537	94.31544	0.14/0.5
8/9	N30C70	1.0	70%	0.32020	0.74714	3.97586	94.95680	0.14/0.5
10	N95C5	2.0	5%	5.77215	0.30380	2.92405	91.00000	0.14
11	N70C30	2.0	30%	2.40491	1.03067	3.47853	93.08589	0.14
12	N30C70	2.0	70%	0.60796	1.41858	3.77443	94.19903	0.14

3. Simulation Methods

Simulations of ignition delay time were performed using the Senkin module in the ANSYS Chemkin-Pro 2022R1 software, employing a constant-volume homogeneous reactor model. This approach is justified because the ignition process behind the reflected shock wave is considered a homogeneous gas-phase reaction. In this study, six reaction mechanisms, including NH_3-C_3H_8, CEU, and Konnov2023, among others, were selected for simulation, and the results were compared with shock-tube experimental data. The details of these reaction mechanisms are listed in Table 3. To accurately investigate the ignition characteristics in the shock tube, numerical simulations of the IDTs for ammonia/propane mixtures were carried out under conditions strictly consistent with the experimental setup.

Table 3. Basic information about the referenced model.

Model	Species	Reactions	Methods-Objects	Years-References
CEU	91	444	Heat flux-LBV	2021 [28]
Wang	188	1604	CVB-LBV	2022 [29]
M-NUIG	356	2309	JSR-NOx	2023 [17]
Konnov2023	498	5719	Heat flux-LBV	2023 [30]
NH_3-C_3H_8	356	2443	Shock tube-IDT	2024 [22]
SJTU2025	612	3335	RCM-IDT	2025 [25]

4. Results and Discussion

4.1. Model Validation

Figure 3 compares the predictive performance of six representative kinetic models from the literature against experimental data. Basic information on these models is provided in Table 2. As observed, different mechanisms exhibit variations in predicting the IDTs of pure ammonia and ammonia/propane blended fuels. The experimental data for pure ammonia are taken from the work of Gao et al. [31].

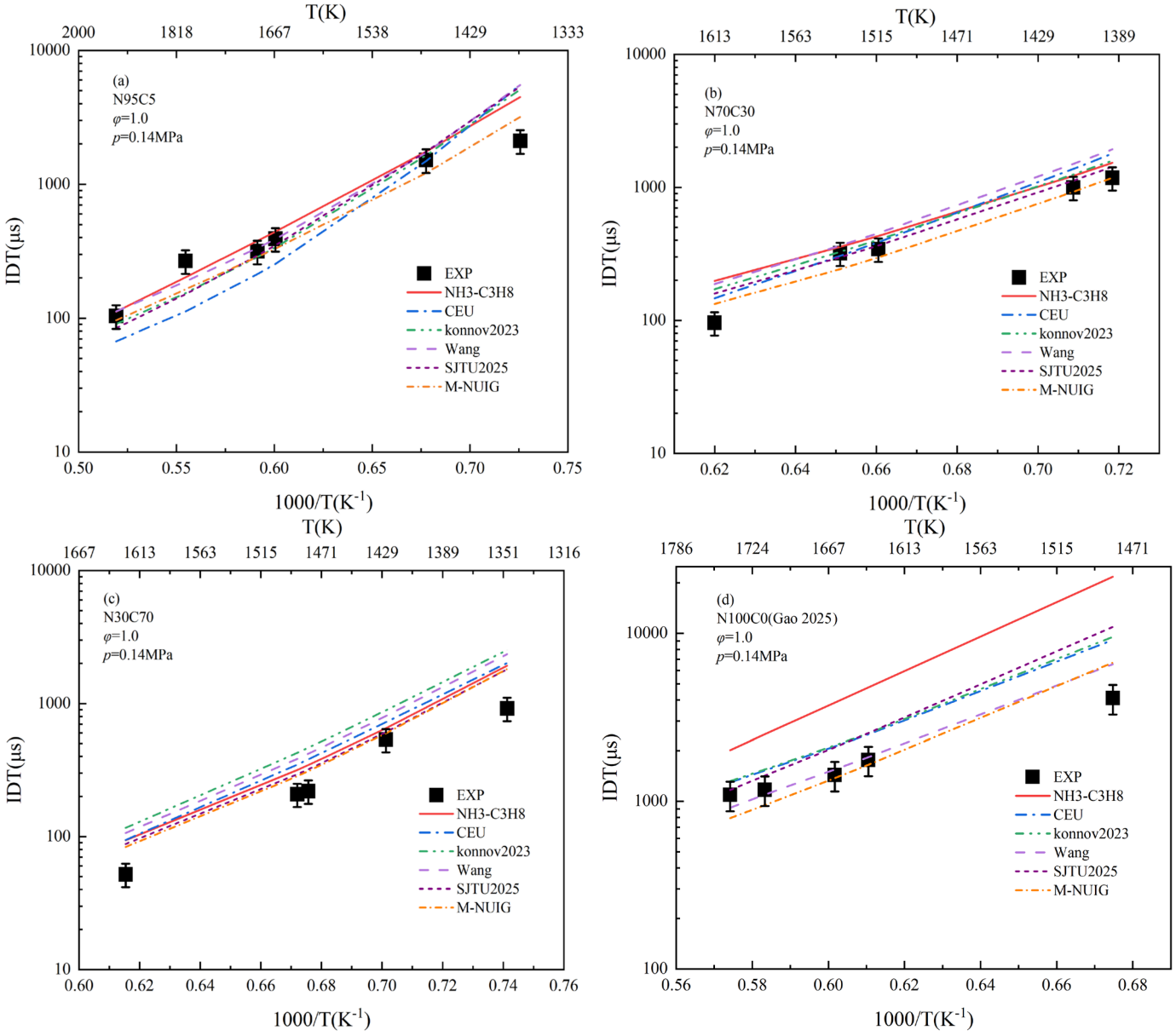


Figure 3. Comparisons of measured and model-predicted IDTs. (**a**) N95C5. (**b**) N70C30. (**c**) N30C70. (**d**) N100C0. (Pure ammonia data from [31]).

Regarding the IDTs of ammonia/propane mixtures, for the N95C5 blend, only the CEU mechanism shows under-prediction at high temperatures. Its hydrocarbon reactions and C–N interaction reactions are adopted from the San Diego mechanism [32] and the Konnov2021 mechanism [33], respectively, with updated rate parameters for the reaction N + NO = N_2 + O. The other five mechanisms provide satisfactory predictions for the IDTs of ammonia/propane at this blending ratio. For the N70C30 mixture, both the

SJTU2025 mechanism and the M-NUIG mechanism exhibit good predictive performance. The SJTU2025 mechanism is constructed based on the POLIMI2023 mechanism [34] and the Aramco3.0 mechanism [35], with additional cross-reaction rates between NH_2 and C_3 alkanes/alkenes. It also incorporates the NH_2 + CH_2O/CH_3CHO reactions emphasized by Shrestha et al. [36]. The predictions of this model show good agreement with experimental data obtained from a rapid compression machine (RCM). The remaining models significantly overestimate the IDTs at low temperatures. For the N30C70 mixture, the predictions of the SJTU2025 and M-NUIG mechanisms are similar and relatively accurate, while the other models generally overpredict the IDTs.

However, significant discrepancies are observed among different mechanisms in predicting the IDTs of pure ammonia. As illustrated in Figure 3d, the Wang mechanism demonstrates the best predictive performance for pure ammonia. This mechanism primarily includes C1–C4 hydrocarbon sub-mechanisms, an NH_3 sub-mechanism, C–N interaction sub-mechanisms, and their mutual couplings. The NH_3 sub-mechanism is based on the study by Zhang et al. [37], which enables accurate prediction of species identification and quantitative analysis for NH_3/H_2 mixtures via Fourier Transform Infrared (FTIR) spectroscopy. The predictions of the M-NUIG mechanism are relatively close to the experimental values, though slightly inferior to those of the Wang mechanism. M-NUIG was developed based on the NUIG mechanism [38], with its NH_3 sub-mechanism also derived from Zhang et al. [37]. However, the rate coefficients for NH_2 + CH_4/C_2H_6 were adopted from Glarborg et al. [39] and updated according to the computational results of Siddiqui et al. [40]. Therefore, both mechanisms provide reasonably accurate predictions for the IDTs of pure ammonia.

Overall, the SJTU2025 model demonstrates the best predictive performance and the M-NUIG model can also provide reasonably accurate predictions for the IDTs of the mixtures. To quantitatively evaluate the predictive capability of the SJTU2025 mechanism, the deviations between the simulated and experimental IDTs were further analyzed. A total of 21 experimental data points with corresponding simulations were considered. The average absolute relative error (AARE) between the simulated and experimental IDTs was 43.55%, while the Pearson correlation coefficient was 0.956. The high correlation coefficient indicates that the SJTU2025 mechanism can effectively capture the overall variation trend of the experimental IDTs. In addition, 90.48% of the simulated IDTs fall within a factor of two of the corresponding experimental values. Nevertheless, a maximum relative error of 166.20% was observed under certain conditions, and the mean signed relative error of 35.25% indicates an overall tendency of the mechanism to overpredict the experimental IDTs. These results suggest that the SJTU2025 mechanism generally reproduces the major trends of the experimental ignition characteristics, although quantitative discrepancies remain under some specific conditions. Although the SJTU2025 model still exhibits certain quantitative prediction deviations under some operating conditions, it is generally able to capture the variation trend of the experimental results. Therefore, this mechanism is selected for further analysis and prediction. (The validation of the SJTU2025 model under other experimental conditions has been added to the Supplementary Materials).

4.2. Effect of the Propane Content

To investigate the effect of propane addition on ammonia ignition, this study measured the IDTs of various NH_3/C_3H_8/O_2/Ar mixtures.

As shown in Figures 4–6, the measured IDTs are plotted as a function of temperature. In the experiments, the mole fraction of C_3H_8 in the NH_3/C_3H_8 fuel mixtures ranged from 5% to 70%, while the overall equivalence ratio of the mixtures varied from 0.5 to 2.0. Figure 4 presents the measured IDTs for stoichiometric NH_3/C_3H_8 mixtures at 0.14 MPa

and 0.5 MPa, accompanied by data for pure NH_3 mixtures from reference [31] for comparative purposes. It can be observed that adding C_3H_8 to ammonia significantly promotes the ignition of NH_3. Under a pressure of 0.14 MPa, the IDT for fuel mixtures containing 5% C_3H_8 is approximately 5 times shorter than that of pure NH_3, and auto-ignition can occur at lower temperatures. Furthermore, compared to the fuel mixture with 5% C_3H_8, the experimental results for NH_3/C_3H_8 blended fuels containing 30% and 70% C_3H_8 shift further toward shorter IDTs. A similar trend can be observed in the experimental results under elevated pressure conditions at 0.5 MPa. As shown in Figure 4b, a notable change is observed for NH_3/C_3H_8 mixtures with low C_3H_8 concentrations. When the C_3H_8 addition increases from 5% to 30%, the IDT decreases by approximately 50% at a temperature of 1450 K. However, under 0.5 MPa, the difference in measured IDTs between fuel mixtures containing 30% and 70% C_3H_8 is relatively small. This indicates that under elevated pressure conditions, especially at higher C_3H_8 concentrations, the effect of C_3H_8 addition on the ignition of NH_3/C_3H_8 fuel mixtures diminishes.

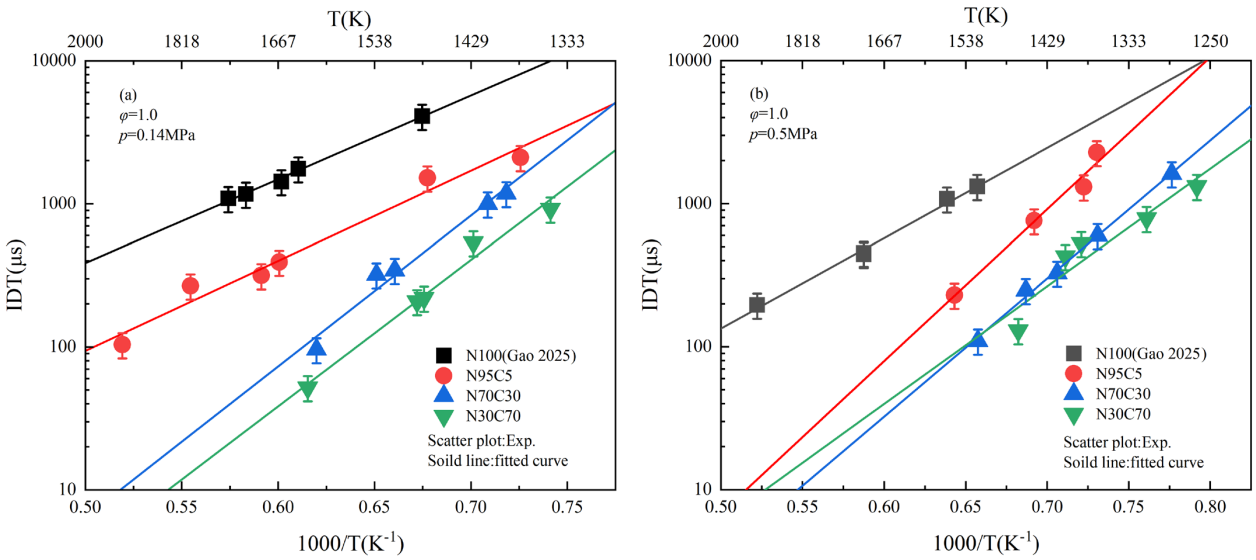


Figure 4. IDTs of NH_3/C_3H_8 mixtures with different C3H8 contents. (**a**) p = 0.14 MPa. (**b**) p = 0.5 MPa. (Pure ammonia data from [31]).

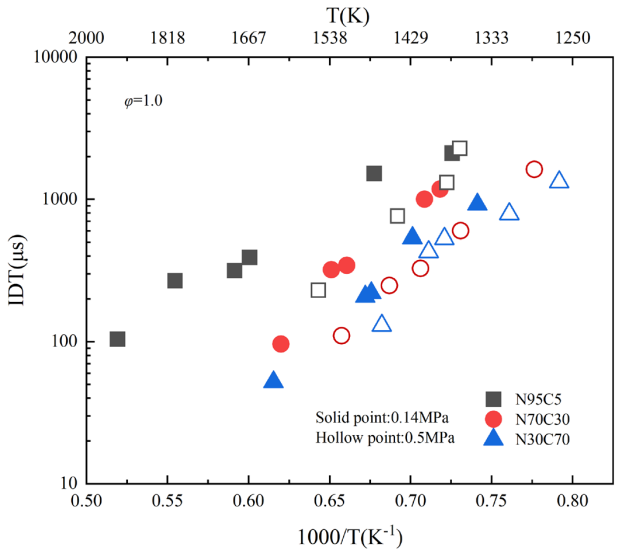


Figure 5. IDTs of NH_3/C_3H_8 mixtures with different pressures.

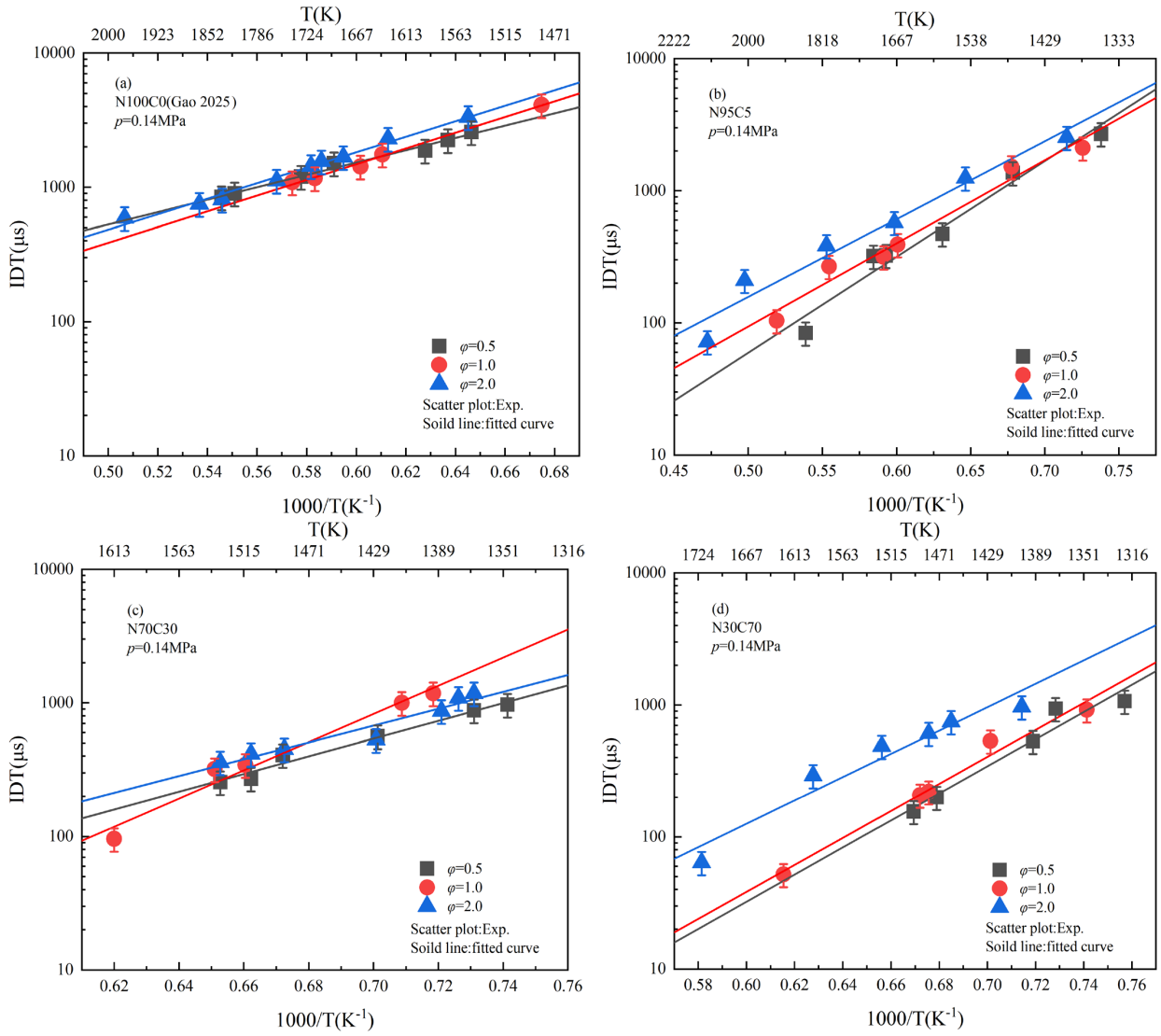


Figure 6. IDTs of NH_3/C_3H_8 mixtures with different equivalence ratios. (**a**) N100C0. (**b**) N95C5. (**c**) N70C30. (**d**) N30C70. (Pure ammonia data from [31]).

4.3. Effect of the Pressure

Figure 5 illustrates the variation of IDTs for different NH_3/C_3H_8 fuel mixtures with pressure under stoichiometric conditions.

As expected, the IDT shortens with increasing pressure. However, in the low-temperature region, the differences in IDTs for the N95C5 mixture under varying pressure conditions are relatively small. For fuel mixtures containing 5% and 30% C_3H_8, a comparison of the measured IDTs at 0.14 MPa and 0.5 MPa reveals that elevated pressure enhances reactivity, resulting in a more than two-fold reduction in IDT. In contrast, for conditions with C_3H_8 concentrations as high as 70%, the IDTs under the two pressure conditions are very similar. This indicates that mixtures with high C_3H_8 content exhibit weaker sensitivity of IDT to pressure variations. It should be noted that these observations are limited to the investigated pressure range of 0.14–0.5 MPa, and further measurements at additional pressure levels are required to establish a more comprehensive pressure dependence.

4.4. Effect of the Equivalence Ratio

As shown in Figure 6, the IDTs of NH_3 blended fuels with varying C_3H_8 contents were measured across equivalence ratios ranging from 0.5 to 2.

From Figure 6a,b, it can be concluded that pure ammonia shows negligible sensitivity to changes in equivalence ratio, whereas the addition of 5% C_3H_8 significantly amplifies the influence of equivalence ratio on the IDT of the mixture. Overall, for all NH_3/C_3H_8 fuel mixtures, the measured IDT increases with increasing equivalence ratio. It can be observed that in the low-temperature region, the variation in IDT caused by different equivalence ratios is relatively small. In Figure 6b,d, it is observed under high-temperature conditions that when the equivalence ratio increases from 0.5 to 1.0, the increase in IDT for the fuel mixtures is less than 10%; however, when the equivalence ratio rises from 1.0 to 2.0, the delay time can increase by more than two-fold. In contrast, the effect of equivalence ratio on fuel mixtures containing 30% C_3H_8 is less pronounced. Experimental observations indicate that for this specific mixture, variations in the equivalence ratio within the range of 0.5 to 2 result in only slight changes in the IDT. Overall, the influence of the equivalence ratio on IDT becomes more pronounced under high-temperature conditions.

5. Chemical Kinetic Analysis

5.1. Sensitivity Analysis

In order to better understand the influence of propane content and temperature variation on the ignition process of NH_3/C_3H_8 mixtures, a forced sensitivity analysis was performed at T = 800 K, 1200 K, and 1600 K, p = 0.14 MPa, and φ = 1.0, as shown in Figure 7. The forced sensitivity coefficient is defined as:

$$S = \frac{\ln(\tau_+/\tau_-)}{\ln(k_+/k_-)} = \frac{\ln(\tau_+/\tau_-)}{\ln(2.0/0.5)} \quad (1)$$

In the equation, τ_+ represents the IDT calculated by doubling the reaction rate constant, while τ_- corresponds to the IDT calculated by halving the rate constant. Here, k_+ denotes twice the reaction rate constant, and k_- denotes half of it. A negative sensitivity coefficient indicates that the reaction has an ignition-promoting effect, whereas a positive sensitivity coefficient suggests an ignition-inhibiting effect.

As shown in Figure 7a, at T = 800 K, R702 (C_3H_8+ HO_2 = IC_3H_7 + H_2O_2) exhibits the highest sensitivity and promotes ignition. Its sensitivity shows a nonlinear relationship with the C_3H_8 content—the higher the C_3H_8 content, the stronger the sensitivity of R702 to the IDT. Meanwhile, the sensitivities of other reactions involving C_3H_8, such as R685 (C_3H_8 + OH = NC_3H_7 + H_2O) and R686 (C_3H_8 + HO_2 = NC_3H_7 + H_2O_2), also show an increasing trend, further promoting the ignition of the mixture. Notably, as the C_3H_8 content increases from 5% to 30%, the sensitivity coefficients of elementary reactions involving reactive nitrogen intermediates such as NH_2, HNO, and NO—including R74, R133, R141, R73, and R26—exhibit a sharp, nonlinear decline. This is because the C–H bonds in propane molecules possess significantly lower bond dissociation energies than the N–H bonds in ammonia molecules. When the propane content increases, the dominant reaction pathway in the mixture shifts from the dehydrogenation of NH_3 to the cracking and dehydrogenation of propane. Radicals such as H, O, and OH preferentially react with propane, generating i-C_3H_7 or n-C_3H_7 radicals, thereby reducing the concentration of NH_2 radicals. The resulting C_3H_7 radicals rapidly undergo β-scission, producing a large number of methyl CH_3 radicals and their subsequent oxidation products (such as HO_2, CH_2O, CO), rather than proceeding through the slower nitrogen-involved chain-branching reactions. Consequently, with increasing propane content, the sensitivity coefficients of carbon-containing reactants such as R702 and R686 rise markedly, whereas those of nitrogen-involved reactions decline sharply due to the drastic drop in both the concentrations of reactants NH_2 and NO and the corresponding reaction fluxes.

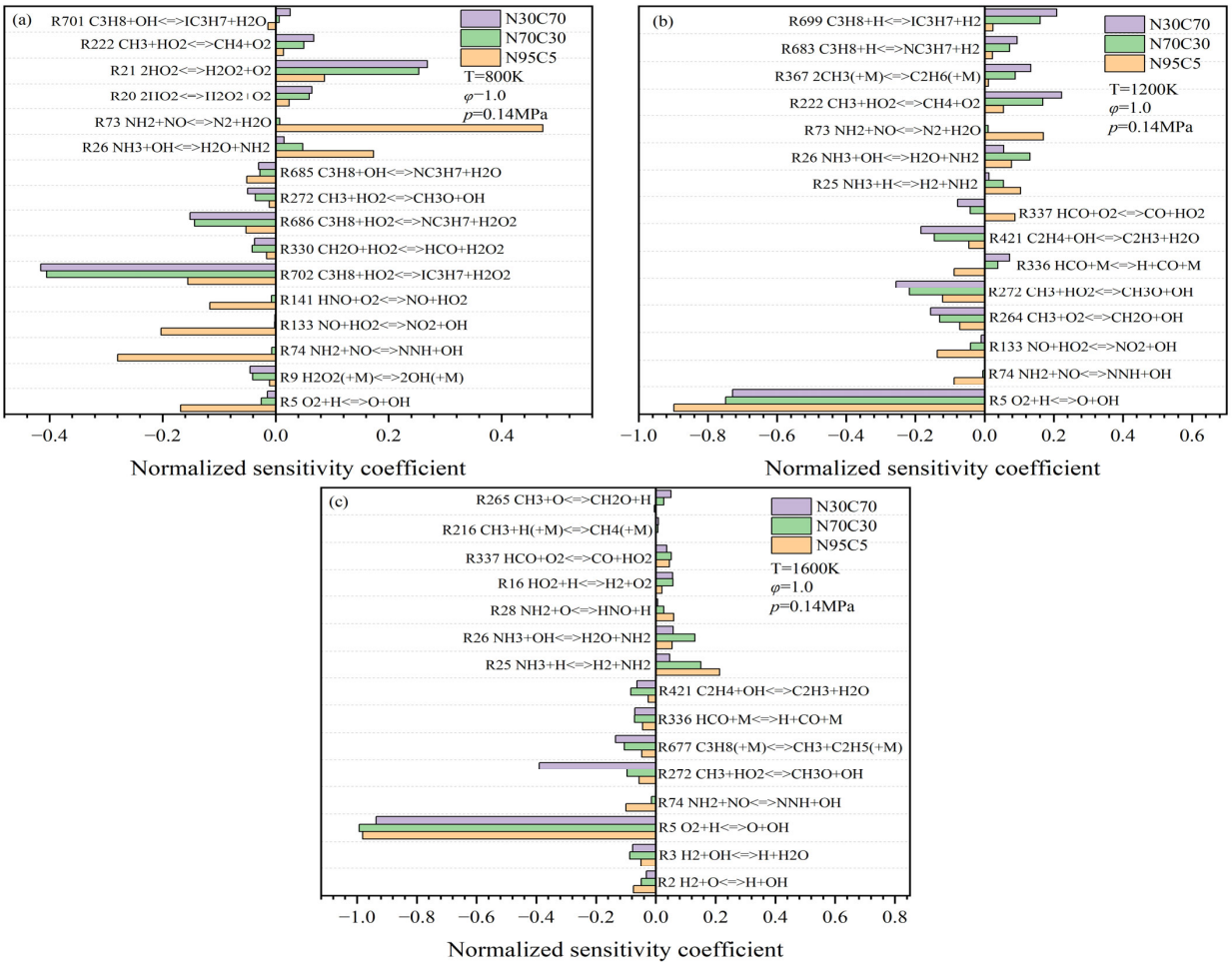


Figure 7. Sensitivity of various blends at different temperatures. (**a**) T = 800 K. (**b**) T = 1200 K. (**c**) T = 1600 K.

At temperatures of T = 1200 K and 1600 K, R5 (O_2 + H = O + OH) exhibits the highest sensitivity and promotes ignition. As shown in Figure 7b, when T = 1200 K, the high-temperature chain-branching reaction R5 shows the greatest sensitivity. Under these conditions, the activity of nitrogen-containing reactions at high temperatures is lower than that at 800 K. Therefore, while the trend of decreasing sensitivity of nitrogen-containing reactions with increasing propane content persists when the C_3H_8 content rises to 30%, the magnitude of this decline is significantly less pronounced compared to that observed at 800 K. Furthermore, the dehydrogenation reactions of C_3H_8, such as R683 (C_3H_8 + H = NC_3H_7 + H_2) and R699 (C_3H_8 + H = IC_3H_7 + H_2), exhibit an ignition-inhibiting effect, with their sensitivity strengthening as the C_3H_8 content increases. This occurs because a higher C_3H_8 content promotes these dehydrogenation reactions, which compete with the highly sensitive high-temperature chain-branching reaction R5 for H radicals. It is noteworthy that among the reactions promoting ignition, CH_3 plays a significant role. Reaction R264 (CH_3 + O_2 = CH_2O + OH) serves as the primary consumption pathway for methyl radicals at high temperatures, generating the active radical OH along with CH_2O. CH_2O is a key intermediate that rapidly yields CO, thereby facilitating exothermic reactions and consequently promoting ignition. Reaction R272 (CH_3+ HO_2 = CH_3O + OH) further contributes by converting the less reactive HO_2 radical into the active OH radical, thereby enriching the active radical pool and enhancing ignition. Additionally, the intermediate HCO warrants attention. As the C_3H_8 content increases from 5% to 30%, reaction R337 (HCO + O_2 = CO + HO_2) initially exhibits an inhibiting effect before shifting to a

promoting one. This occurs because, at low C_3H_8 levels, this reaction converts the relatively reactive HCO into the less reactive HO_2, thereby suppressing ignition. However, when the C_3H_8 content rises, the concentration of HO_2 in the radical pool increases, which in turn inhibits the conversion of HCO to HO_2. Consequently, a higher C_3H_8 content promotes ignition through this pathway. On the other hand, reaction R336 (HCO + M = H + CO + M) shows a trend that shifts from promotion to inhibition. This is because the pyrolysis of HCO generates H radicals, which accelerate ignition. Yet, an increase in C_3H_8 content elevates the concentration of H radicals, thereby inhibiting the progress of R336 and resulting in an overall ignition-inhibiting effect.

At T = 1600 K, R5 exhibits the highest sensitivity and promotes ignition. Under high-temperature conditions, the activity of nitrogen-containing reactions is further reduced; consequently, their sensitivity coefficients show little variation with increasing C_3H_8 content. The sensitivity coefficient of the high-temperature chain-branching reaction R5 displays a trend of initially increasing and then decreasing as the C_3H_8 content rises. This occurs because when the propane content increases from 5% to 30%, thermal decomposition reactions such as R677 ($C_3H_8 + M = CH_3 + C_2H_5 + M$) are promoted, generating substantial amounts of CH_3 and C_2H_5 radicals. These alkyl radicals further produce active H radicals, thereby enhancing the progress of reaction R5. When the propane content rises from 30% to 70%, the increased ignition-promoting sensitivity of reaction R677 under these conditions leads to extensive pyrolysis of propane at ultra-high temperatures and blending ratios, producing a large quantity of CH_3 radicals. The high concentration of CH_3 radicals further reacts via R272 to generate active OH radicals. The elevated concentration of OH radicals, in turn, exerts an inhibitory effect on the progress of reaction R5. This explains why the sensitivity of R5 first rises and then declines with increasing C_3H_8 concentration. It also accounts for the notable increase in the sensitivity of reaction R272 when the C_3H_8 content reaches 70% compared to that at 30%.

In summary, temperature plays a decisive role in the ignition kinetics of NH_3/C_3H_8 mixtures. In the intermediate temperature regime of 800 K, the addition of C_3H_8 leads to a sharp decline in the sensitivity of nitrogen-containing reactions by competing with ammonia for reaction pathways. As the temperature rises to 1200 K and 1600 K, the decrease in sensitivity of nitrogen-containing reactions becomes notably more gradual, indicating that elevated temperatures systematically diminish the activity and importance of nitrogen-related chemistry. Meanwhile, the sensitivity of the core chain-branching reaction $H + O_2 = O + OH$ exhibits a complex coupling effect between temperature and blending ratio. At 1200 K, it shows the highest sensitivity and decreases monotonically with increasing propane content, whereas at 1600 K, it follows a non-monotonic trend—first rising and then falling. This reveals the critical regulatory role of the dynamic balance between H-atom production and consumption under high-temperature conditions in the ignition process.

5.2. Reaction Pathway Analysis

Figure 8 presents the main reaction pathways for the three mixtures—N95C5, N70C30, and N30C70—at T = 1600 K, p = 0.14 MPa, and φ = 1.0, with the analysis conducted when 20% of the initial NH_3 has been consumed. A reaction flux-based pathway analysis was employed to identify the dominant consumption and formation routes of key nitrogen- and carbon-containing species. Specifically, the reaction flux of each elementary reaction in the SJTU2025 mechanism was evaluated at the selected reaction state, and the contribution of an individual reaction pathway was determined by normalizing its flux with respect to the total consumption or formation flux of the corresponding target species. Only the major reaction pathways contributing to the evolution of the key species are presented in Figure 8.

The black, red, and blue pathways represent N95C5, N70C30, and N30C70, respectively. This analysis enables a direct comparison of the dominant reaction pathways among mixtures with different NH_3/C_3H_8 ratios. As shown in Figure 8a, within this reaction network, NH_3 is primarily consumed via H-abstraction reactions involving OH, O, and H radicals, producing NH_2 radicals. Among these, the reaction $NH_3 + OH = NH_2 + H_2O$ serves as the dominant consumption pathway for NH_3, accounting for approximately 50% of the total NH_3 consumption. The NH_2 radicals generated from the dehydrogenation of NH_3 exhibit high reactivity and can further react with H radicals to form NH radicals. Additionally, interactions between NH_2 radicals can consume NH_2 via the reaction $2NH_2 = NH_3 + NH$, producing NH radicals and regenerating NH_3. NH radicals then undergo radical recombination with NH_2 through the reaction $NH_2 + NH = N_2H_2 + H$, yielding N_2H_2. N_2H_2 is readily hydrogenated by H or NH_2, or decomposes via pyrolysis to release H-atoms, ultimately converting into NNH radicals. NNH subsequently decomposes once more to form the stable N_2 molecule.

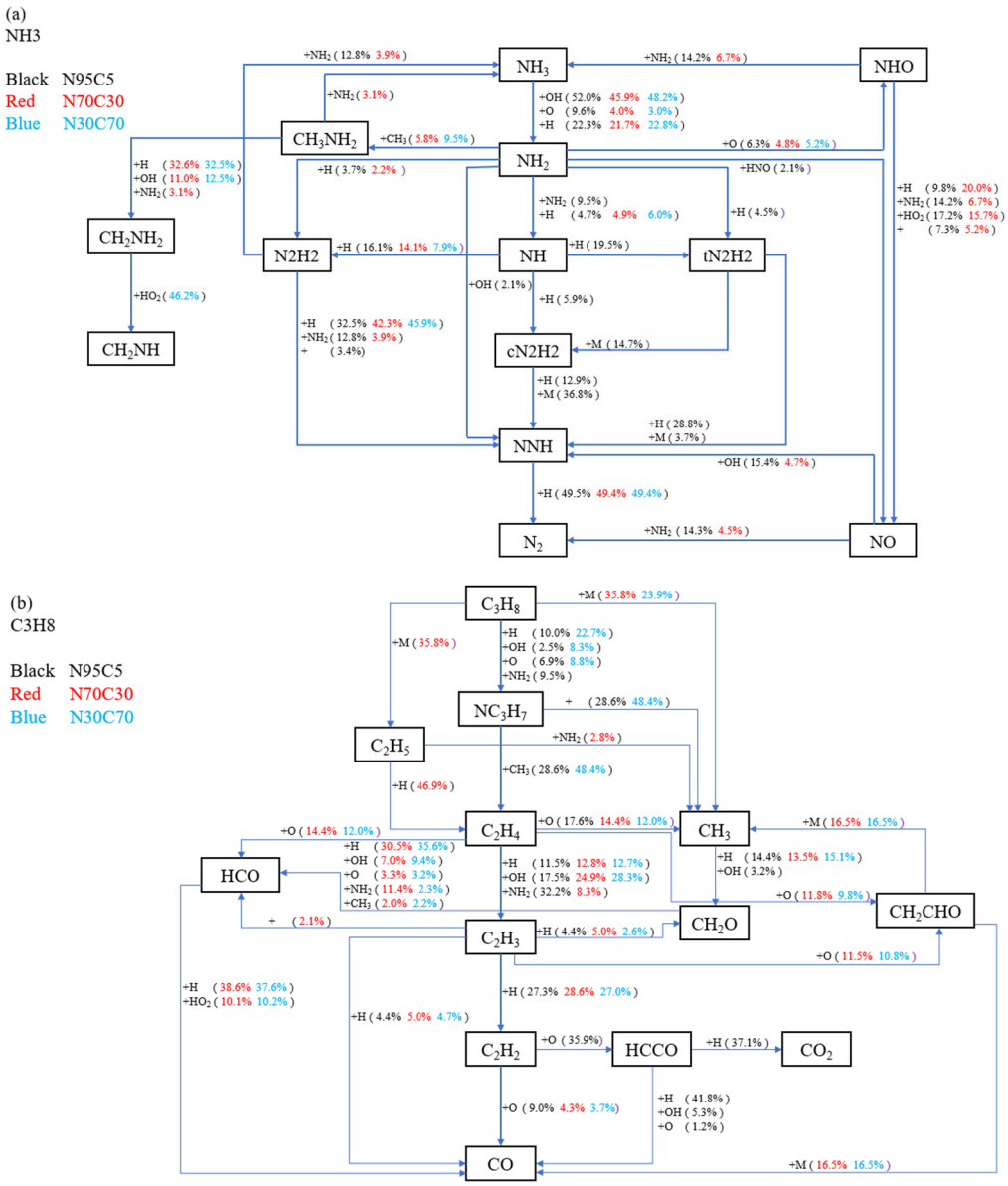


Figure 8. The reaction pathways of various mixtures under the conditions of 1600 K, 0.14 MPa, φ = 1.0 and 20% NH3 consumption. (**a**) NH_3. (**b**) C_3H_8.

For the N95C5 fuel blend, the primary reaction pathway for NH_3 consumption is $NH_3 \rightarrow NH_2 \rightarrow NH \rightarrow N_2H_2(\rightarrow cN_2H_2/tN_2H_2) \rightarrow NNH \rightarrow N_2$. It is worth noting that in this mixture, the reaction path involves the conversion of NH radicals into both cis- and trans-N_2H_2 isomers. This occurs because the propane content is low, and nitrogen-containing reactions dominate the chemistry under these conditions. When the C_3H_8 content increases to 30%, a new consumption pathway emerges for NH_3: $NH_3 \rightarrow NH_2 \rightarrow CH_3NH_2 \rightarrow CH_2NH_2$. Due to the higher propane content, CH_3 radicals—key intermediates from C_3H_8—react with NH_2 radicals to form the C–N cross-species CH_3NH_2. This species further reacts with active radicals such as H, OH, and NH_2 to regenerate NH_3 and produce another C–N cross-species, CH_2NH_2. When the propane content reaches 70%, CH_2NH_2 further undergoes a dehydrogenation reaction with O_2 to produce CH_2NH. Notably, as the propane content increases, the competition between C-containing radicals and N-containing radicals weakens the conversion of N-containing radicals to NO, thereby effectively reducing NO formation.

Figure 8b illustrates the reaction pathways of C_3H_8 under the same conditions. C_3H_8 is primarily consumed via two main routes:

1. $C_3H_8 \rightarrow NC_3H_7 \rightarrow C_2H_4 \rightarrow C_2H_3 \rightarrow C_2H_2 \rightarrow CO$.
2. $C_3H_8 \rightarrow C_2H_5 \rightarrow C_2H_4 \rightarrow C_2H_3 \rightarrow C_2H_2 \rightarrow CO$.

When the C_3H_8 content is 5%, the reaction pathway corresponds to route 1. Under these conditions, the chemistry is dominated by NH_3. High-temperature decomposition of NH_3 generates active H radicals and NH_2 radicals, with NH_2 further reacting to produce O and OH radicals. Consequently, C_3H_8 is primarily consumed through dehydrogenation reactions involving H, O, and OH radicals, yielding NC_3H_7 radicals. NC_3H_7 then decomposes to yield C_2H_4, which subsequently reacts with radicals to form C_2H_3. At this stage, ammonia decomposition serves as the primary source of radicals, while hydrocarbon reactions play a secondary role.

When the C_3H_8 content increases to 30%, third-body reactions gradually replace dehydrogenation as the primary consumption pathway for C_3H_8, shifting the reaction route to path 2. The higher concentration of C_3H_8 dilutes the influence of ammonia on the radical pool, leading to a decrease in the concentration of H radicals. Under these conditions, C_3H_8 mainly decomposes via third-body effects to generate active CH_3 radicals and C_2H_5 radicals. The C_2H_5 radicals then undergo a C–N cross-reaction with NH_2 radicals to form CH_3NH_2. This indicates that at 30% C_3H_8 content, the influence of third-body reactions outweighs that of H, O, and OH initiated hydrogen abstraction, thereby giving rise to a new reaction pathway.

However, it is noteworthy that when the C_3H_8 content increases to 70%, the reaction pathway of C_3H_8 reverts to route 1. The consumption of H, O, and OH radicals in the pathway gradually rises, indicating that hydrogen-abstraction reactions regain a larger share. Meanwhile, the consumption of NH_2 radicals decreases significantly, suggesting that the system has shifted from an NH_2-generation-dominated stage to an NH_2-consumption-dominated stage. The influence of primary NH_3 decomposition on the radical pool weakens, which implies that the reaction has entered a phase dominated by deeper conversion of nitrogen species and oxidation of hydrocarbon intermediates. Notably, as the C_3H_8 concentration increases, substantial amounts of H radicals are generated via the dehydrogenation reaction $C_3H_8 \rightarrow NC_3H_7 + H$, while pyrolysis and oxidation of C_3H_8 also contribute significantly to the production of O and OH radicals in the radical pool. Simultaneously, the concentration of C_2H_4 rises markedly, and C_2H_4 serves as an important precursor to CH_2O. Under these conditions, a new oxidation pathway emerges: $C_2H_4 \rightarrow CH_3(\rightarrow HCO) \rightarrow CH_2O \rightarrow HCO \rightarrow CO$. Among these steps, $HCO + O_2 = CO + HO_2$ is highly exothermic, which accelerates temperature-sensitive reactions and concurrently produces HO_2 radicals.

These HO_2 radicals can further participate in chain-branching reactions, thereby increasing the propagation rate of the chain reactions and ultimately promoting ignition.

5.3. Rate-of-Production Analysis

Rate-of-production (ROP) analysis of NH_3 was conducted under the conditions of T = 1600 K, p = 0.14 MPa, and φ = 1.0. The results are shown in Figure 9a–d. As illustrated in Figure 9a, during the initial stage of the reaction, due to the absence of radicals at the start, R24 ($NH_3 = NH_2 + H$) serves as the primary consumption pathway for NH_3. Its consumption rate remains essentially constant over time, and this reaction produces active H radicals, providing the initial buildup of the radical pool. The consumption rates of all other elementary reactions involving NH_3 begin from zero and gradually increase. Among the pathways where NH_3 is consumed via radical dehydrogenation, R26 ($NH_3 + OH = H_2O + NH_2$) is the primary consumption route, followed by R27 ($NH_3 + O = NH_2 + OH$) and R25 ($NH_3 + H = H_2 + NH_2$). These three chain-initiating reactions generate active NH_2 and OH radicals, thereby enriching the radical pool. Additionally, under the current scale of coordinates, the consumption rate of NH_3 by R37 ($NH_2 + NH = NH_3 + N$) is almost negligible. As the reaction proceeds, the consumption of NH_3 by H gradually exceeds that by O. As ignition approaches, R26 remains the primary consumption pathway for NH_3, followed by R25 and R27. It is worth noting that the generated NH_2 radicals can reform NH_3 via reaction R41 ($2NH_2 = NH_3 + NH$), which acts as a reaction that inhibits NH_3 consumption.

As shown in Figure 9b, due to the higher reactivity of C_3H_8 compared to NH_3, adding only 5% C_3H_8 can generate a greater variety of active species during the early stage of the reaction, thereby initiating chain reactions more efficiently. This significantly enhances the consumption rates of R25, R26, and R27. It is noteworthy, however, that the addition of C_3H_8 increases the concentrations of H and OH radicals in the radical pool. As a result, in the initial reaction stage, the consumption rate of NH_3 via R25 exceeds that via R26, unlike in the case of pure ammonia. CH_3 is a key intermediate from C_3H_8 decomposition; therefore, the dehydrogenation reaction R3280 ($NH_2 + CH_4 = NH_3 + CH_3$) cannot be ignored in NH_3 consumption, with its consumption rate comparable to that of R27 during the initial reaction stage. In the early phase, NH_2 radicals produced from NH_3 dehydrogenation can react with HNO radicals and CH_2O (an intermediate from C_3H_8) to regenerate NH_3, thereby continuously inhibiting NH_3 consumption throughout the reaction. Among these, reaction R3283 ($NH_2 + CH_2O = HCO + NH_3$) exhibits the strongest inhibitory effect on NH_3 consumption. However, as the concentration of NH_2 radicals increases, the inhibitory effect of reaction R41 eventually surpasses that of R3283. As ignition approaches, the consumption of NH_3 by OH consistently exceeds that by H. Moreover, near the moment of ignition, the primary consumption pathways for NH_3 remain consistent with those observed for pure ammonia in Figure 8a. Although the peak values of R26, R25, and R27 increase, their order of magnitude remains unchanged.

As shown in Figure 9c,d, the results indicate that with an increase in C_3H_8 content, the reactions promoting NH_3 decomposition during the initial stage remain consistent with those observed for the 5% C_3H_8 case in Figure 9b. Notably, due to the elevated C_3H_8 content, the concentrations of HO_2 radicals and C_2H_4—an intermediate from C_3H_8—rise. Among the reactions that inhibit NH_3 consumption, the roles of R3282 ($NH_2 + C_2H_4 = NH_3 + C_2H_3$) and R3289 ($NH_2 + HO_2 = NH_3 + O_2$) become more pronounced compared to cases with lower C_3H_8 content. Near the ignition moment, the primary consumption pathways of NH_3 remain consistent with those shown in Figure 9b. However, the peak values of R26, R25, and R27 appear earlier in time and are somewhat reduced in magnitude. It is noteworthy that in the three mixtures with different C_3H_8 con-

tents, the net consumption rate of NH_3 exhibits a declining trend to varying degrees during the initial stage. The higher the C_3H_8 content, the more pronounced this trend becomes. This occurs because, at this stage, the increased concentration of C_3H_8-related intermediate species leads to a higher reaction rate for their recombination with NH_2 to regenerate NH_3, surpassing the rate of NH_3 consumption. As the reaction progresses, the concentrations of H, O, and OH radicals in the radical pool rise, significantly accelerating the consumption of NH_3 via reactions R26, R25, and R27. Consequently, the net consumption rate returns to an upward trend as the reaction proceeds.

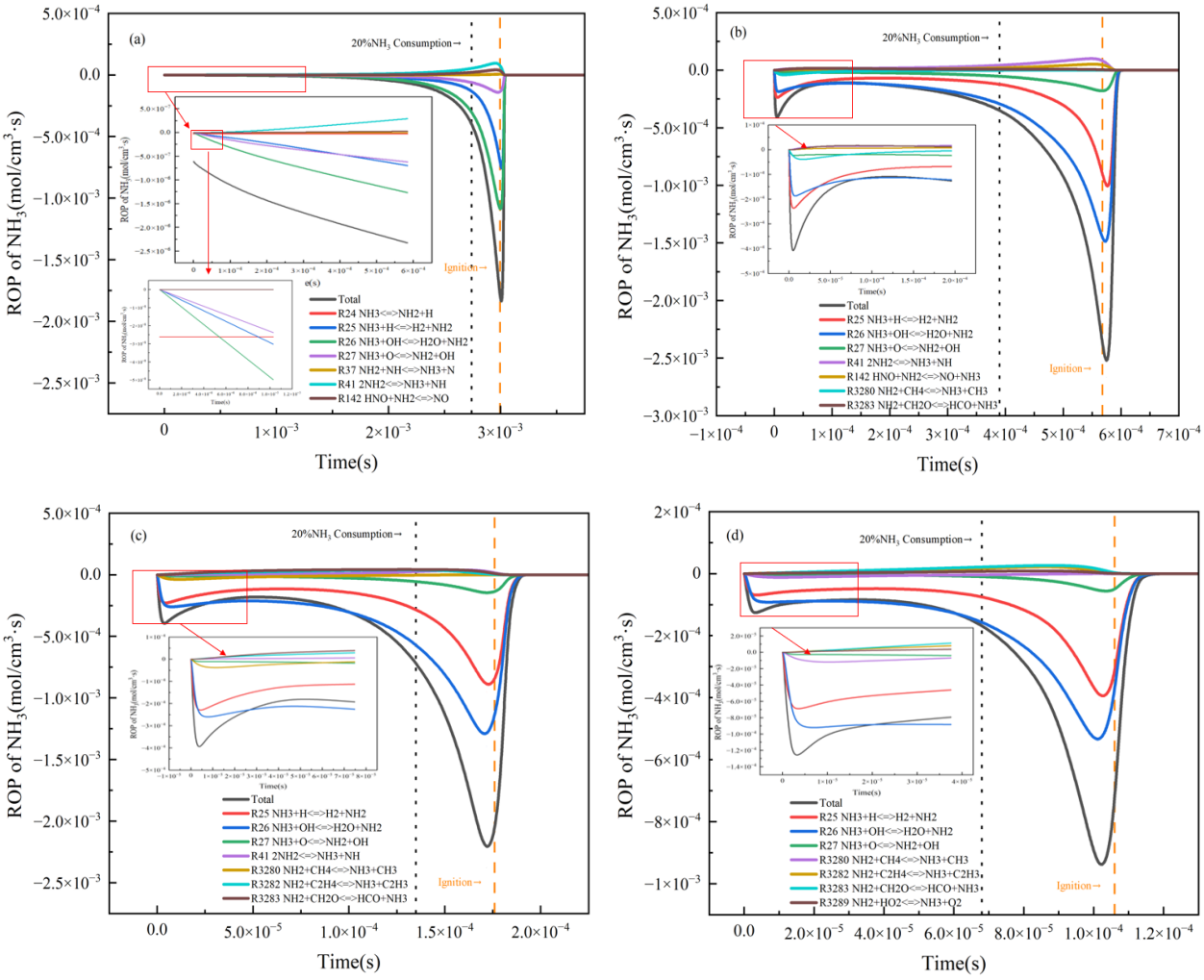


Figure 9. ROP of NH_3. (**a**) N100C0. (**b**) N95C5. (**c**) N70C30. (**d**) N30C70.

6. Conclusions

In this study, shock tube experiments were conducted to systematically measure the IDTs of NH_3/C_3H_8 mixtures across a wide range of parameters (T = 1263–2117 K, p = 0.14 and 0.5 MPa, φ = 0.5, 1.0 and 2.0, with C_3H_8 blending ratios of 5%, 30%, and 70%). These measurements, for the first time, extend the range of operating conditions beyond those in previous studies. Furthermore, detailed kinetic analyses were performed using existing chemical kinetic models to investigate the auto-ignition characteristics of NH_3/C_3H_8 mixtures. The main conclusions are summarized as follows:

The addition of C_3H_8 substantially shortens the IDT of NH_3/C_3H_8 mixtures, with the strongest promoting effect observed at 5% C_3H_8. As the C_3H_8 fraction increases from 30% to 70%, the IDT-shortening effect gradually weakens. Increasing pressure from

0.14 to 0.5 MPa generally reduces the IDT, whereas propane-rich mixtures exhibit weaker pressure sensitivity. The effect of equivalence ratio is relatively small between φ = 0.5 and 1.0 but becomes more pronounced between φ = 1.0 and 2.0, particularly for the 70% C_3H_8 mixture.

Sensitivity analysis indicates that the dominant ignition-controlling reactions change with temperature and C_3H_8 content. At low temperature, R702 (C_3H_8 + HO_2 = i-C_3H_7 + H_2O_2) is the dominant ignition-promoting reaction, highlighting the importance of C_3H_8/HO_2 chemistry. With increasing temperature, the dominant promoting reaction shifts to R5 (O_2 + H = O + OH), reflecting the increasing importance of chain-branching chemistry. Meanwhile, the sensitivity of nitrogen-containing reactions decreases markedly with increasing C_3H_8 content at 800 K, while this effect becomes less pronounced at higher temperatures.

Reaction pathway analysis shows that C_3H_8 addition does not fundamentally change the dominant NH_3-to-N_2 oxidation pathway, which proceeds mainly through NH_3 → NH_2 → NH → N_2H_2 → NNH → N_2. The initial consumption of NH_3 is dominated by H-abstraction reactions, particularly NH_3 + OH = NH_2 + H_2O. The subsequent conversion of NH_2 through reactions with NH/H radicals promotes the formation of N_2H_2 and NNH, ultimately leading to N_2 formation. When the C_3H_8 content exceeds 30%, however, an additional C–N coupling pathway becomes important, in which CH_3 radicals derived from C_3H_8 oxidation react with NH_2 to form CH_3NH_2, thereby introducing an additional interaction between the carbon and nitrogen reaction networks.

The dominant fuel-consumption characteristics also depend on the C_3H_8 blending ratio. For N95C5 and N30C70, fuel consumption is mainly promoted by H-abstraction/dehydrogenation reactions involving active radicals, whereas N70C30 is more strongly affected by thermal decomposition through third-body reactions. These results demonstrate that the ignition behavior of NH_3/C_3H_8 mixtures is governed by the competition between C_3H_8 oxidation, NH_3-to-N_2 conversion, and C–N coupling chemistry, with their relative contributions varying with temperature and mixture composition.

Supplementary Materials: The following supporting information can be downloaded at: https://www.mdpi.com/article/10.3390/pr14182953/s1. References [41–43] are cited in Supplementary Materials.

Author Contributions: Conceptualization, H.X. and C.W.; methodology, D.G. and W.M.; software, D.G. and W.M.; validation, D.G. and J.L. formal analysis, H.X.; investigation, H.X. and Y.G.; resources, A.C.; data curation, D.G. and W.M.; writing—original draft preparation, D.G.; writing—review and editing, H.X. and Y.N.; visualization, J.L. and C.W.; supervision, A.C. and H.X.; project administration, A.C. and H.X.; funding acquisition, A.C. and Y.N. All authors have read and agreed to the published version of the manuscript.

Funding: This research was funded by the Guangzhou Education Bureau's 2024 University Research Project (Project No. 2024312536), Hunan Provincial Science and Technology Innovation Program (Project No. 2024AQ2013) and Scientific Research Capacity Improvement Project of Key Construction Discipline of Guangdong Province (Project No. 2022ZDJS099).

Data Availability Statement: The original contributions presented in this study are included in the article. Further inquiries can be directed to the corresponding authors.

Acknowledgments: Special thanks are given to those who participated in the writing of this paper. We acknowledge Xianglin Chu and Xin Li for their technical support during the data collection process.

Conflicts of Interest: The authors declare no conflicts of interest.

References

1. Valera-Medina, A.; Xiao, H.; Owen-Jones, M.; David, W.; Bowen, P. Ammonia for power. *Prog. Energy Combust. Sci.* **2018**, *69*, 63–102. [CrossRef]
2. Elbaz, A.M.; Wang, S.; Guiberti, T.F.; Roberts, W.L. Review on the recent advances on ammonia combustion from the fundamentals to the applications. *Fuel Commun.* **2022**, *10*, 100053. [CrossRef]
3. Valera-Medina, A.; Amer-Hatem, F.; Azad, A.K.; Dedoussi, I.C.; de Joannon, M.; Fernandes, R.X.; Glarborg, P.; Hashemi, H.; He, X.; Mashruk, S.; et al. Review on ammonia as a potential fuel: From synthesis to economics. *Energy Fuels* **2021**, *35*, 6964–7029. [CrossRef]
4. Dimitriou, P.; Javaid, R. A review of ammonia as a compression ignition engine fuel. *Int. J. Hydrogen Energy* **2020**, *45*, 7098–7118. [CrossRef]
5. Kobayashi, H.; Hayakawa, A.; Somarathne, K.D.K.A.; Okafor, E.C. Science and technology of ammonia combustion. *Proc. Combust. Inst.* **2019**, *37*, 109–133. [CrossRef]
6. Li, T.; Duan, Y.; Wang, Y.; Zhou, M.; Duan, L. Research progress of ammonia combustion toward low carbon energy. *Fuel Process. Technol.* **2023**, *248*, 107821. [CrossRef]
7. Zhang, Y.; Zhou, W.; Liang, Y.; Yu, L.; Lu, X. An experimental and detailed kinetic modeling study of the auto-ignition of NH3/diesel mixtures: Part 1-NH3 substitution ratio from 20% to 90%. *Combust. Flame* **2023**, *251*, 112391. [CrossRef]
8. Zheng, L.; Mi, S.; Li, H.; Tan, X.; Qian, Y.; Feng, M.; Lu, X. Experimental study on the combustion and emission characteristics of ammonia-diesel dual fuel engine under high ammonia energy ratio conditions. *J. Energy Inst.* **2024**, *114*, 101557. [CrossRef]
9. Wang, Z.; Ji, C.; Zhang, T.; Wang, S.; Yang, H.; Zhai, Y.; Yang, J. Experimental study on the combustion of NH3/H2/air based on the passive turbulent jet ignition. *Fuel* **2024**, *365*, 131268. [CrossRef]
10. Dai, L.; Gersen, S.; Glarborg, P.; Mokhov, A.; Levinsky, H. Autoignition studies of NH3/CH4 mixtures at high pressure. *Combust. Flame* **2020**, *218*, 19–26. [CrossRef]
11. Sun, J.; Yang, Q.; Zhao, N.; Chen, M.; Zheng, H. Numerically study of CH4/NH3 combustion characteristics in an industrial gas turbine combustor based on a reduced mechanism. *Fuel* **2022**, *327*, 124897. [CrossRef]
12. Yu, M.; Luo, G.; Sun, R.; Qiu, W.; Chen, L.; Wang, L.; Hu, Z.; Li, X.; Yao, H. Experimental and numerical study on emission characteristics of NH3/DME/air flames in a premixed burner. *Combust. Flame* **2024**, *259*, 113098. [CrossRef]
13. Dai, L.; Hashemi, H.; Glarborg, P.; Gersen, S.; Marshall, P.; Mokhov, A.; Levinsky, H. Ignition delay times of NH3/DME blends at high pressure and low DME fraction: RCM experiments and simulations. *Combust. Flame* **2021**, *227*, 120–134. [CrossRef]
14. Li, X.; Ma, Z.; Jin, Y.; Wang, X.; Xi, Z.; Hu, S.; Chu, X. Effect of methanol blending on the high-temperature auto-ignition of ammonia: An experimental and modeling study. *Fuel* **2023**, *339*, 126911. [CrossRef]
15. Li, M.; Zhu, D.; He, X.; Moshammer, K.; Fernandes, R.; Shu, B. Experimental and kinetic modeling study on auto-ignition properties of ammonia/ethanol blends at intermediate temperatures and high pressures. *Proc. Combust. Inst.* **2023**, *39*, 511–519. [CrossRef]
16. Gao, P.; Gao, Z.; Ma, Z.; Li, X.; Chu, X.; Wang, X.; Zhao, K. An experimental and kinetic modeling study on the auto-ignition of ammonia/butan-1-ol mixtures. *Fuel* **2025**, *382*, 133741. [CrossRef]
17. Yin, G.; Xiao, B.; Zhan, H.; Hu, E.; Huang, Z. Chemical kinetic study of ammonia with propane on combustion control and NO formation. *Combust. Flame* **2023**, *249*, 112617. [CrossRef]
18. Yin, G.; Xiao, B.; You, J.; Zhan, H.; Hu, E.; Huang, Z. Experimental and kinetic modeling study on propane enhancing the laminar flame speeds of ammonia. *Fuel Process. Technol.* **2023**, *247*, 107779. [CrossRef]
19. Cheng, B.; Zhu, Y.H.; Zhang, F.; Wang, P.P.; Chen, P. Study on co-firing characteristics and NOx emission of ammonia/propane. *J. Phys. Conf. Ser. IOP Publ.* **2022**, *2208*, 012011. [CrossRef]
20. Chen, C.; Wang, Z.; Yu, Z.; Han, X.; He, Y.; Zhu, Y.; Konnov, A.A. Experimental and kinetic modeling study of laminar burning velocity enhancement by ozone additive in NH_3+O_2+N_2 and NH_3+CH_4/C_2H_6/C_3H_8+ air flames. *Proc. Combust. Inst.* **2023**, *39*, 4237–4246. [CrossRef]
21. Wang, Z.; Ji, C.; Wang, D.; Zhang, T.; Zhai, Y.; Wang, S. Experimental and numerical study on laminar burning velocity and premixed combustion characteristics of NH_3/C_3H_8/air mixtures. *Fuel* **2023**, *331*, 125936. [CrossRef]
22. Liu, J.; Liu, D.; Dai, L.; Zou, C.; Lin, Q.; Peng, C. The effects of C/N cross-reactions on the NH_3/C_3H_8 combustion: A shock-tube and modeling study. *Combust. Flame* **2024**, *270*, 113716. [CrossRef]
23. Nobakht, A.; Cepeda, F.; Karataş, A.E. Pressure effects on soot formation and maturity in propane–ammonia diffusion flames. *Proc. Combust. Inst.* **2026**, *42*, 106105. [CrossRef]
24. Lin, H.; Zhang, K.; Jiang, X.; Gao, W.; Cheng, X.; Dong, S. An experimental and numerical study of the auto-ignition characteristics of ammonia/propane blends. *Fuel* **2026**, *409*, 137774. [CrossRef]
25. Liang, Y.; Wang, Z.; Yu, L.; Lu, X. Experimental and kinetic insight on auto-ignition process of ammonia/propane mixture: Focus on oxygen effect. *Combust. Flame* **2026**, *283*, 114572. [CrossRef]

26. Jin, Y.; Li, X.; Wang, X.; Ma, Z.; Chu, X. Effect of dimethyl ether on ignition characteristics of ammonia and chemical kinetics. *Fuel* **2023**, *343*, 127885. [CrossRef]
27. Chu, X.; Li, X.; Gao, P.; Ma, Z.; Xiao, H.; Xie, C.; Zhang, Z.; Wang, X. High-temperature auto-ignition characteristics of NH_3-H_2-CH_4. *Fuel* **2024**, *365*, 131228. [CrossRef]
28. Wang, Z.; Han, X.; He, Y.; Zhu, R.; Zhu, Y.; Zhou, Z.; Cen, K. Experimental and kinetic study on the laminar burning velocities of NH_3 mixing with CH_3OH and C_2H_5OH in premixed flames. *Combust. Flame* **2021**, *229*, 111392. [CrossRef]
29. Wang, D.; Wang, Z.; Zhang, T.; Zhai, Y.; Hou, R.; Tian, Z.-Y.; Ji, C. A comparative study on the laminar C1–C4 n-alkane/NH3 premixed flame. *Fuel* **2022**, *324*, 124732. [CrossRef]
30. Konnov, A.A.; Chen, J.; Lavadera, M.L. Measurements of the laminar burning velocities of small alkyl esters using the heat flux method: A comparative study. *Combust. Flame* **2023**, *255*, 112922. [CrossRef]
31. Gao, P.; Ma, Z.; Xie, C.; Qu, P.; Zhang, Z.; Wang, X. Effect of butan-1-ol on autoignition characteristics of ammonia. *Fuel* **2025**, *401*, 135871. [CrossRef]
32. U. Mechanism, Chemical-Kinetic Mechanisms for Combustion Applications, Mechanical and Aerospace Engineering (Combustion Research), University of California at San Diego. Available online: https://web.eng.ucsd.edu/mae/groups/combustion/mechanism.html (accessed on 5 July 2026).
33. Han, X.; Lavadera, M.L.; Brackmann, C.; Wang, Z.; He, Y.; Konnov, A.A. Experimental and kinetic modeling study of NO formation in premixed CH_4+O_2+N_2 flames. *Combust. Flame* **2021**, *223*, 349–360. [CrossRef]
34. Stagni, A.; Arunthanayothin, S.; Dehue, M.; Herbinet, O.; Battin-Leclerc, F.; Bréquigny, P.; Mounaïm-Rousselle, C.; Faravelli, T. Low-and intermediate-temperature ammonia/hydrogen oxidation in a flow reactor: Experiments and a wide-range kinetic modeling. *Chem. Eng. J.* **2023**, *471*, 144577. [CrossRef]
35. Zhou, C.-W.; Li, Y.; Burke, U.; Banyon, C.; Somers, K.P.; Ding, S.; Khan, S.; Hargis, J.W.; Sikes, T.; Mathieu, O.; et al. An experimental and chemical kinetic modeling study of 1, 3-butadiene combustion: Ignition delay time and laminar flame speed measurements. *Combust. Flame* **2018**, *197*, 423–438. [CrossRef]
36. Shrestha, K.P.; Mai, T.V.; Giri, S.; Reddy, V.M.; Szőri, M.; Verma, R.; Mauss, F.; Giri, B.R.; Huynh, L.K. Reaction Kinetics of NH2 With H2CO and CH3CHO: Modeling Implications for NH3-Dual Fuel Blends. *Int. J. Chem. Kinet.* **2025**, *57*, 403–416. [CrossRef]
37. Zhang, X.; Moosakutty, S.P.; Rajan, R.P.; Younes, M.; Sarathy, S.M. Combustion chemistry of ammonia/hydrogen mixtures: Jet-stirred reactor measurements and comprehensive kinetic modeling. *Combust. Flame* **2021**, *234*, 111653. [CrossRef]
38. Wu, Y.; Panigrahy, S.; Sahu, A.B.; Bariki, C.; Beeckmann, J.; Liang, J.; Mohamed, A.A.; Dong, S.; Tang, C.; Pitsch, H.; et al. Understanding the antagonistic effect of methanol as a component in surrogate fuel models: A case study of methanol/n-heptane mixtures. *Combust. Flame* **2021**, *226*, 229–242. [CrossRef]
39. Glarborg, P.; Miller, J.A.; Ruscic, B.; Klippenstein, S.J. Modeling nitrogen chemistry in combustion. *Prog. Energy Combust. Sci.* **2018**, *67*, 31–68. [CrossRef]
40. Siddique, K.; Altarawneh, M.; Gore, J.; Westmoreland, P.R.; Dlugogorski, B.Z. Hydrogen abstraction from hydrocarbons by NH2. *J. Phys. Chem. A* **2017**, *121*, 2221–2231. [CrossRef]
41. Petersen, E.L.; Rickard, M.J.A.; Crofton, M.W.; Abbey, E.D.; Traum, M.J.; Kalitan, D.M. A facility for gas-and condensed-phase measurements behind shock waves. *Meas. Sci. Technol.* **2005**, *16*, 1716–1729. [CrossRef]
42. Li, X.; Chu, X.; Xiao, H.; Chen, H.; Ma, Z.; Wang, X.; Hu, S.; Xi, Z. Shock tube and modeling study on autoignition properties of ammonia/diethyl ether mixtures at high temperatures. *Fuel* **2024**, *368*, 131653. [CrossRef]
43. Aronowitz, D.; Santoro, R.J.; Dryer, F.L.; Glassman, I. Kinetics of the oxidation of methanol: Experimental results semi-global modeling and mechanistic concepts. *Symp. (Int.) Combust.* **1979**, *17*, 633–644. [CrossRef]

Disclaimer/Publisher's Note: The statements, opinions and data contained in all publications are solely those of the individual author(s) and contributor(s) and not of MDPI and/or the editor(s). MDPI and/or the editor(s) disclaim responsibility for any injury to people or property resulting from any ideas, methods, instructions or products referred to in the content.